



Characterization of Mk-IV and EBR-II X441A Metallic Fuel Pins for the THOR-C-2 and THOR-M-TOP-1 Experiments

August 2023

*Results from Post-Transient Neutron
Tomography of THOR-C-2 Capsule and Pre-
transient Non-Destructive and Destructive
Examination of DP 36 and DP 40*

Allison Probert, Luca Capriotti, and Jason Schulthess
Idaho National Laboratory



DISCLAIMER

This information was prepared as an account of work sponsored by an agency of the U.S. Government. Neither the U.S. Government nor any agency thereof, nor any of their employees, makes any warranty, expressed or implied, or assumes any legal liability or responsibility for the accuracy, completeness, or usefulness, of any information, apparatus, product, or process disclosed, or represents that its use would not infringe privately owned rights. References herein to any specific commercial product, process, or service by trade name, trade mark, manufacturer, or otherwise, does not necessarily constitute or imply its endorsement, recommendation, or favoring by the U.S. Government or any agency thereof. The views and opinions of authors expressed herein do not necessarily state or reflect those of the U.S. Government or any agency thereof.

Characterization of Mk-IV and EBR-II X441A Metallic Fuel Pins for the THOR-C-2 and THOR-M-TOP-1 Experiments

**Results from Post-Transient Neutron Tomography of THOR-C-2
Capsule and Pre-transient Non-Destructive and Destructive
Examination of DP 36 and DP 40**

**Allison Probert, Luca Capriotti, and Jason Schulthess
Idaho National Laboratory**

August 2023

**Idaho National Laboratory
Idaho Falls, Idaho 83415**

<http://www.inl.gov>

**Prepared for the
U.S. Department of Energy
Office of Nuclear Energy
Under DOE Idaho Operations Office
Contract DE-AC07-05ID14517**

Page intentionally left blank

SUMMARY

Current interest in sodium-cooled fast reactor designs, such as TerraPower's Natrium Reactor, has highlighted the need for advanced-reactor fuel technology development. A Fuel Safety Research and Development (FSRD) program for metallic fast reactor fuels has been created to achieve comprehensive safety testing within the re-commissioned Transient Reactor Test (TREAT) facility at the Idaho National Laboratory.

Despite over 60 years of metallic fuel irradiation, some uncertainties exist in the performance of the fuel system, particularly under anticipated operational occurrences and severe accident scenarios. Throughout historical testing within the Experimental Breeder Reactor (EBR)-II and the Fast Flux Test Facility, fuel behavior has demonstrated benign response to transient reactor conditions; however, accurate predictions of failure thresholds depend on several factors meriting further study.

In advancing the FSRD program, two planned transient heating experiments are at various stages of completion. The Temperature Heat sink Overpower Response (THOR)-C-2, fueled with an fresh Mk-IV U-10Zr pin, has undergone transient irradiation in TREAT and post-transient three-dimensional neutron tomography. Additionally, pre-transient characterization of test and sibling U-19Pu-10Zr pins for THOR-M-TOP-1 was performed by both non-destructive and destructive methods. The test and sibling pins were selected from previously irradiated EBR-II experiment X441A. Both pins underwent visual examination, precise gamma spectrometry, two-dimensional neutron radiography, and element contact profilometry while the sibling pin was additionally subjected to sectioning and optical microscopy.

THOR-C-2 radiography captured the fuel and cladding relocation during the intermediate transient at the top and bottom of the THOR capsule, allowing key features to be linked to the pin's measured thermal response. For THOR-M-TOP-1, a solid baseline for steady-state behavior has been established. No anomalous features were identified in either the test or sibling pin. Defining characteristics and features were recorded for further comparisons.

Page intentionally left blank

CONTENTS

SUMMARY	iii
ACRONYMS.....	viii
1. INTRODUCTION.....	1
1.1. Metallic Fuels.....	1
1.2. Historical Safety Testing.....	1
1.3. THOR-C-2 Background and Motivation	6
1.4. THOR-M-TOP-1 Background and Motivation.....	6
2. SUMMARY OF PRE-TRANSIENT CHARACTERIZATION, EXPERIMENTS, AND IRRADIATION HISTORY	7
2.1. Pre-Transient Characterization.....	7
2.2. Experiment Description and Sample Information.....	7
2.2.1. THOR-C-2 Irradiation Plan	7
2.2.2. THOR-M-TOP-1 Irradiation Plan.....	8
3. NON-DESTRUCTIVE EXAMINATION RESULTS AND DISCUSSION.....	9
3.1. Visual Inspection.....	9
3.2. Neutron Radiography	10
3.3. Dimensional Inspection.....	11
3.4. Gamma Spectrometry	13
4. DESTRUCTIVE EXAMINATION RESULTS AND DISCUSSION.....	14
4.1. Fission-Gas Release	14
4.2. Sectioning.....	14
4.3. Metallography	14
5. POST-TRANSIENT ANALYSIS OF COMISSIONING TOP TEST.....	17
5.1. Neutron Computed Tomography	17
5.2. Thermal Measurements.....	19
6. FUTURE WORK.....	20
7. CONCLUSIONS.....	20
8. ACKNOWLEDGEMENT	21
9. REFERENCES.....	21

FIGURES

Figure 1. Targeted transient for the THOR-C-2 experiment in the TREAT facility [47]......	8
---	---

Figure 2. Through-window visual image of DP 40 with wire wrap (left) and VEM image of DP 40 without wire wrap (right).....	10
Figure 3. Thermal neutron radiography of the fuel elements DP 36 (top) and DP 40 (bottom).....	11
Figure 4. Thermal neutron radiograph of low-density and fluff-structure regions at the tops of the fuel columns of DP 36 (left) and DP 40(right).	11
Figure 5. Diametral measurements from element contact profilometry for DP 40 (top) and DP 36 (bottom). Axial position is measured from the bottom of the fuel pin.	12
Figure 6. Axial distribution of Cs-137 as detected by gamma scan, overlaid with neutron radiographs of X441A-DP 36 (top) and X441A-DP 40 (bottom).	13
Figure 7. DP 36 fuel-pin cutting diagram, describing the different sample configurations, purposes, and axial positions.	14
Figure 8. Transverse optical metallography cross-sections of X441A-DP 36 taken at (a) 0.25x/L, (b) 0.50x/L, and (c) 0.98x/L.....	16
Figure 9. 3D nCT projection of the lower region of interest for THOR-C-2 (a), individual nCT slices showing three thermocouple placements within the Ti heatsink at each of the axial positions (b) 4.1 cm, (c) 8.3 cm, and (d) 12.5 cm, and accompanying heat sink temperatures measured from TCs at axial positions (e) 4.1 cm, (f) 8.3 cm, and (g) 12.5 cm.....	17
Figure 10. 3D nCT projection of the upper region of interest for THOR-C-2, (a) individual nCT slices showing three thermocouple placements within the Ti heatsink at each of the axial positions (b) 29.7 cm, (c) 25.4 cm, and (d) 23.9 cm, and accompanying heat sink temperatures measured from the TCs at axial positions (e) 29.7 cm, (f) 25.4 cm, and (g) 21.1 cm.....	18
Figure 11. Transverse nCT radiographs showing breached cladding at (a) 30.0 cm, (b) central void at 5.3 cm, and © relocated fuel at 0.7 cm above the beginning of the fuel column.	18
Figure 12. Cladding strain measurements from nCT for (a) the lower and (b) upper ROIs.	19

TABLES

Table 1. Diffusion couples and associated melting eutectic temperatures for HT9-clad U-Pu-Zr system.	3
Table 2. OPT-1 pin specifications and experiment parameters.	4
Table 3. M-Series pin specifications and test parameters.	5
Table 4. THOR-MTOP-1 and sibling pin test matrix.	7
Table 5. Summary of Pre-Transient Characterization Completed on DP 40 and DP 36.	7
Table 6. Geometry and specifications for Mk-IV fuel pin used in THOR-C-2.	8
Table 7. Geometry and specifications for DP 40 and DP 36.	9
Table 8. Measured axial growth for Pins DP 40 and DP 36.	11
Table 9. Maximum cladding deformation measured via contact profilometry.....	12

Page intentionally left blank

ACRONYMS

AES	Acoustic-emission sensor
ALMR	Advanced Liquid Metal Fuel Reactor
AOO	Anticipated operational occurrence
BU	Burnup
DBA	Design-basis accident
DE	Destructive examination
DOE	Department of Energy
EBR-II	Experimental Breeder Reactor II
ECP	Element-contact profilometry
FCCI	Fuel cladding chemical interaction
FCMI	Fuel cladding mechanical interaction
FFTF	Fast Flux Test Facility
FSRD	Fuels safety research and development
FGR	Fission-gas release
GASR	Gas Assay, Sample, and Recharge (System)
HFEF	Hot Fuel Examination Facility
IFR	Integral Fast Reactor
INL	Idaho National Laboratory
LFA	Laser Flash Analysis
LOF	Loss of Flow
LOHS	Loss of heat sink
LVDT	Linear variable differential transformer
MARCH	Minimal activation retrievable capsule holder
MFC	Materials and Fuels Complex
MFF	Mechanistic fuel failure
MOX	Mixed oxide fuel
nCT	Neutron computed tomography
NDE	Non-destructive examination
NRAD	Neutron Radiography Reactor

PPS	Plant-protection system
RIP	Rod internal pressure
RSWF	Radioactive Scrap and Waste Facility
OPT	OverPower transient
PGS	Precision gamma scanner
ROI	Region of interest
SFR	Sodium-cooled Fast Reactor
SHRT	Sudden heat removal testing
TC	Thermocouple
THOR	Temperature Heat sink Overpower Response
TOP	Transient overpower
TREAT	Transient Reactor Test
VEM	Visual examination machine

Page intentionally left blank

Characterization of Mk-IV and EBR-II X441A Metallic Fuel Pins for the THOR-C-2 and THOR-M-TOP-1 Experiments

1. INTRODUCTION

1.1. Metallic Fuels

Metallic fuels have been examined for use in fast reactors for over 60 years [1]. Adopting the fuel system would assist in long-term actinide management, require easy and cost-competitive fabrication, and offer a closed fuel cycle with minimized threat from proliferation [2, 3]. However, early attention was redirected to mixed oxide (MOX) fuel as the priority fuel for fast reactors due to issues with fuel-cladding mechanical interaction (FCMI), resulting in low achievable burnup in uranium-based metallic fuels [3]. The lifetime limiting behaviors were the result of high fuel swelling and the formation of a low-melting-point eutectic at the fuel-cladding interface, exacerbated by high coolant-outlet temperatures in early fast-reactor designs [4]. Expanded testing campaigns with varied pin geometries and metallic alloys revealed key insights into the thermomechanical behavior of metallic fuels, resulting in an improved pin design and fuel composition [5–7]. These enhanced pin designs are primary candidates for use in sodium-cooled fast reactors (SFRs) and boast high fuel-utilization capacity, increased fuel-cladding compatibility, and improved safety through inherent feedback mechanisms [2]. Nevertheless, the fuel system also demonstrates behaviors that, when exacerbated under accident conditions, necessitate operational limitations to avoid pin failure [4]; thus, research efforts are needed to compile a comprehensive safe-operating envelope for SFR metallic-fuel qualification.

1.2. Historical Safety Testing

Leading the initiative for metallic-fuel development, Experimental Breeder Reactor (EBR)-II headed many efforts for demonstration of irradiation behavior and assembly of a safety envelope for qualification. To expand its own driver-fuel utilization and meet the demands of many innovative reactor designs—the Fast Flux Test Facility (FFTF), Liquid Metal Fast Breeder Reactor, Clinch River Breeder Reactor, Integral Fast Reactor (IFR), and others—modern metallic alloys U-Zr and U-Pu-Zr were developed, replacing U-Fs. These binary and ternary alloys demonstrated improved irradiation behavior (reaching burnups up to 20 at.%), increased solidus temperature, and lessened fuel/cladding interdiffusion [8, 9]. Furthermore, pin design shifted to employ ferritic/martensitic HT9 stainless steel cladding for its low swelling properties and desirable irradiation-creep resistance [10, 11]. The steady-state performance and high-burnup capability of U-Zr clad in HT9 and U-Pu-Zr clad in D9/HT9 has been thoroughly evaluated in experiments X419–X421, X425, X429, X430, and X447–X451 [3, 12, 13]. Experiment X441 sought to examine the effects of Zr content, plenum-to-fuel volume ratio, fuel smeared density, and cladding thickness on failure due to fuel-cladding chemical interaction (FCCI) U-Pu-Zr fuel pins encased in HT9/D9 cladding. It serves as a benchmark for metallic fuel performance code, LIFE-METAL [5]. Sixty-one pins were irradiated up to a peak burnup of 12.7%, and while no pin breach occurred, post-irradiation examination confirmed the need for major changes to pin design to mitigate life-limiting behaviors, including increasing plenum-to-fuel volume ratio, cladding thickness, and fuel-cladding gap. Increasing the plenum size relative to the metallic fuel-slug volume accommodates fission-gas release (FGR) for rods reaching higher burnups, maintains acceptable internal-pin pressures, and minimizes diametric strain on the cladding [14]. The widening of the fuel-cladding gap, reducing smeared density to 75%, allowed fuel to reach maximum radial expansion contemporaneously with the time at which the fuel and cladding meet, mitigating FCMI and cladding strain [15–17].

The resiliency of the modern metallic fuel system was further demonstrated through high-power and high-temperature testing efforts aimed at qualifying U-Zr as the driver fuel for the IFR and Advanced Liquid Metal Fuel Reactor (ALMR) designs. The IFR-1 and MFF Test series were conducted within the FFTF to identify possible effects of a taller fuel-stack length (36 in. fuel column for the FFTF [18]) on the irradiation performance of metallic rods compared to those tested in EBR-II (13.5 in. fuel column [5]), drawing comparisons largely from EBR-II experiment X447. The IFR-1 experiment examined the behavior of 169 fuel pins irradiated up to 10 at.% burnup over six FFTF operating cycles, reaching a peak power of 40 kW/m and a peak cladding temperature of 608°C [19]. Of those pins, 18 U-19Pu-Zr, 19 U-8Pu-10Zr, and 18 U-Zr pins, all clad in D9, were examined using both non-destructive and destructive techniques. No pin failures were observed throughout the experiment; primarily, all results were consistent with previous EBR-II irradiations of shorter pins with flat power profiles except for the axial location of greatest FCCI formation. Peak FCCI in the IFR-1 pins was observed at approximately $0.7 \times$ length of the pin, corresponding to the point of greatest pin power, rather than peak cladding temperature, and an overall change in fission-product distribution as a result of a longer fuel stack. Further elevated-temperature testing was conducted on segments of an IFR-1 U-19Pu-10Zr pin to examine eutectic's melting under accident conditions [20]. Results were then compared to similar linear heat-ramp testing conducted on EBR-II pins, showing lower-temperature melting occurred in regions of greatest power for longer fuel columns, as opposed to regions of peak cladding temperature for shorter pins.

In the MFF test series, seven sodium-bonded U-Zr-fueled, HT9-clad assemblies were irradiated to a peak linear power up to 59.1 kW/m and reached peak cladding temperatures up to 649°C. No cladding breaches were detected for any of the MFF pins irradiated up to approximately 15.2 at.% burnup, despite the aggressive conditions [18]. The MFF-3 and MFF-5 assemblies experienced the highest peak power and cladding temperatures; thus, four pins from each assembly were selected for detailed post-irradiation examination, including neutron radiography, visual examination, precision gamma spectrometry (PGS), and dimensional analysis [21]. One pin from each assembly also underwent fission-gas pressure and composition, burnup, and metallography analysis. Notable divergences from previously reported behavior of metallic fuels include diminished axial fuel swelling, emergence of a double peak in axial strain in the highest burnup MFF-3 pin, and peak FCCI occurring below the top of the fuel column. The changes demonstrated dependence on fuel geometry, burnup, the reactor's thermal-hydraulic conditions, and thermomechanical behavior of HT9 [21,22].

Although the steady-state irradiation performance of modern metallic fuels is well characterized [3,12,13], full understanding of its behavior during some anticipated operational occurrences (AOOs) remains insufficient. One DBA for SFRs, and the primary focus of this experimental analysis, is a transient overpower (TOP) accident. A TOP features an increase in activity, most probably due to a control-rod withdrawal or failure to insert, but also occurring from the formation of a gas bubble in the core or by core distortion [23]. Other DBAs that generate comparable reactor conditions include a loss of flow (LOF) accident, in which coolant pumps fail or are impaired, and a loss of heat sink (LOHS) accident, in which the heat-transport systems fail. In order to qualify the U-Zr/U-Pu-Zr/HT9 fuel system, the failure mechanisms and thresholds of the fuel pins through both normal conditions, AOOs, and DBAs must be fully understood and adequately assessable through modeling and simulation [24]. The objectives in setting operational limits are to maintain pin integrity and prevent cladding breach, expulsion of fission products, and possible damage to the core.

While still in commission, EBR-II also worked synergistically with the Transient Reactor Test (TREAT) facility to test metallic and oxide fuels across a broad range of the power conditions expected in a TOP occurrence. Under the severe conditions studied throughout historical safety testing of metallic fuels, two central mechanisms of failure have been observed: internal-pressure rupture and cladding attack [25]. In pressure-induced rupture, fuel swelling and FGR cause contact between fuel and cladding, and FCMI strains the cladding and compromises cladding integrity. Improperly accommodating fuel swelling and FGR in fuel-pin design aggravates FCMI. In the cladding-attack failure mechanism, attack

on cladding integrity through the formation of a molten eutectic phase at the fuel-clad interface is influenced by constituent redistribution and FCCI. A comprehensive understanding of the mechanisms behind eutectic formation, constituent redistribution, FCCI, FCMI, and FGR is paramount to predicting cladding strain and wastage-layer formation rate. Moreover, the benign behavior of modern metallic fuel has been emphasized in historical safety testing. In-pile monitoring of fuel behavior during transients—such as fuel motion observed using TREAT’s fast neutron hodoscope—has shown axial fuel extrusion prior to failure, displacing the fuel, reducing reactivity and, in many cases, automatically shutting down the reactor [26]. Additionally, in the event of pin failure, expelled fuel demonstrated excellent compatibility with coolant, and breached cladding remained in similar condition, with no further aggravated burst openings [27].

As previously mentioned, adjustments have been made to the pin design and materials used to minimize cladding strain and wastage, but they are not eliminated; thus, they are still a key focus in safety testing. Furthermore, transient behavior and contributions to these phenomena are additive to steady-state operation behaviors and must be considered in establishing operations limits. Largely, the irradiation and accident behavior of U-Zr/U-Pu-Zr has been inferred from safety testing or driver-fuel qualification examinations conducted with other metallic alloys (U-Fs, where Fs is an equilibrium concentration of metallic fission products resulting from reprocessing), thermal-hydraulic conditions, or nuclear environments [3]. Still, even under extreme conditions, metallic fuels have historically demonstrated benign behavior, and corresponding results can be used to predict and supplement current testing efforts. In developing and qualifying Mk-II, U-Fs driver fuel for EBR-II, transient testing was conducted in-pile and out-of-pile, including subjecting fuel pins to multiple transients during which no cladding breaches occurred [28]. In the 1980s, Argonne National Laboratory expanded its LOF safety-testing efforts through the Shutdown Heat Removal Testing (SHRT) [29,30]. Several tests were conducted on U-Fs driver fuel simulating a severe LOF where coolant circulation was halted within EBR-II, including an unprotected LOF scenario. SHRT-17 demonstrated the effectiveness of the plant-protection system (PPS) as forced coolant circulation was stopped, the reactor was scrammed, and the measured temperatures of the coolant and cladding were within acceptable operational limits throughout the transient.

Similarly, SHRT-45 ceased forced coolant flow but also deactivated the PPS, effectively inhibiting all control-rod insertion. Although temperatures were climbing during the resulting transient, again they stayed within set limits, and inherent feedback mechanisms eventually shut the reactor down. Furthermore, in advancing the conversion of the EBR-II core to Mk-V U-Pu-Zr driver fuel, hot-cell heater testing was conducted in the whole-pin furnace to examine the influence of creep and FCCI during LOF conditions [31]. In test FM-5, a U-20Pu-10Zr pin irradiated up to 10.0 at.% was heated to a peak temperature of 776°C, followed by a rapid decrease to 660°C. During that time, the cladding remained intact, with negligible deformation, and post-test destructive examination showed no fuel melting at the location of peak temperature, demonstrating Mk-V’s capacity to endure a conservative range of LOF thermal conditions. Tests FM-2 and FM-4 were designed to determine the margin to failure of low- and high-burnup Mk-V fuel. The low-burnup fuel pin (FM-2) was heated and held at 820°C for 112 minutes before cladding burst while the high-burnup fuel pin (FM-4) was heated and held at 770°C for 68 minutes before pin rupture. Post-test examination from FM-2 attributed pin failure to FCCI at the location of the burst that had severely thinned cladding, caused a decrease in solidus temperature, and resulted in molten fuel at the interface. Relevant eutectic compositions and temperatures for U-Pu-Zr/HT9 system have been presented in Table 1. Additionally, the pin from FM-4 burst at the plenum due to creep rupture aggravated by rod internal pressure (RIP). However, the pins displayed a significant safety margin to increased temperatures above the typical timing of an LOF event (~2 minutes). Additionally, up-to-date experimentally known properties of U-Pu-Zr and U-Zr systems, including phase transitions and temperature thresholds, have been compiled in various reviews [32–34].

Table 1. Diffusion couples and associated melting eutectic temperatures for HT9-clad U-Pu-Zr system.

Eutectic Composition	Melting Point (°C)	Reference
----------------------	--------------------	-----------

U-U ₆ Fe (3.8 at. % Fe)	810	[35]
U ₆ Fe – U ₂ Fe (10.2 at. % Fe)	725	[35]
U ₂ Fe – Fe (52 at. % Fe)	1080	[35]
U-Cr (20 at. % Cr)	859	[36]
Pu ₆ Fe-PuFe ₂ (10 at. % Fe)	410	[36]
Zr ₃ Fe-Zr ₂ Fe	928	[35]
ZrFe ₃ -Fe	1337	[35]

While the early metallic-fuel safety-testing results provide a general sense of the U-Pu-Zr/U-Zr's benign behavior under accident conditions, modern ternary and binary fuels exhibit specific issues that require an individualized approach [15,20,37–39]. The previously conducted TOP and LOF tests on metallic fuels were limited in samples, instrumentation, and representative experimental conditions, thus rendering the U-Pu-Zr TOP database incomplete and the U-Zr TOP database almost nonexistent. Landmark TOP testing conducted on U-Zr/U-Pu-Zr clad in HT9/D9 includes the EBR-II-based Overpower Transient-1 (OPT-1) experiment and the TREAT-based M-Series tests. In OPT-1, the behavior of 19 EBR-II fuel pins, pre-irradiated during the DP 1 steady-state test, was examined under relatively slow-ramp transient (0.1% $\Delta P/P_0/s$) [40]. Additional pin details and experiment parameters are found in Table 2. A wide range of post-transient characterization was completed on the test pins, revealing no cladding breach or pin failures up to 1.32 times nominal power. Measurements from neutron radiography conducted on the pins showed typical axial elongation, but no permanent deformation to fuel column; pre- and post-transient element contact profilometry showed no additional cladding strain was achieved during the slow-ramp conditions. Finally, destructive sectioning and optical metallography revealed no significant contribution to FCCI, constituent redistribution, or similar behaviors lowering the margin to failure.

Table 2. OPT-1 pin specifications and experiment parameters.

Pin ID	Comp.	Clad	Sm. Dens. (% Theor.)	Burnup (BU) (at.%)	Pre-cond. LHGR (kW/m)	Transient LHGR (kW/m)
DP 55	U-19Pu-10Zr	HT9	75	11.1	41.7	54.8
DP 59	U-19Pu-10Zr	HT9	75	5.5	45.3	59.6
DP 34	U-19Pu-10Zr	HT9	75	5.5	46.0	60.6
DP 35	U-19Pu-10Zr	HT9	75	11.4	41.9	55.2
DP 37	U-19Pu-10Zr	HT9	75	11.3	41.8	55.0
DP 41	U-19Pu-10Zr	HT9	75	11.0	42.0	55.3
DP 25	U-19Pu-6Zr	HT9	75	9.8	42.9	56.5
DP 26	U-19Pu-6Zr	HT9	75	9.7	43.0	56.6
DP 30	U-19Pu-14Zr	HT9	75	12.7	42.5	55.9
DP 31	U-19Pu-14Zr	HT9	75	12.4	42.8	56.3
DP 43	U-19Pu-10Zr	HT9	85	9.9	43.0	56.6
DP 46	U-19Pu-10Zr	HT9	85	4.9	46.8	61.5
DP 49	U-19Pu-10Zr	HT9	85	9.8	43.1	56.7
DP 64	U-19Pu-10Zr	HT9	70	11.8	41.4	54.5
DP 65	U-19Pu-10Zr	HT9	70	6.0	45.3	59.6

Pin ID	Comp.	Clad	Sm. Dens. (% Theor.)	Burnup (BU) (at.%)	Pre-cond. LHGR (kW/m)	Transient LHGR (kW/m)
G308	U-10Zr	HT9	75	8.7	37.6	49.5
G303	U-10Zr	HT9	75	8.6	37.8	49.8
J571	U-10Zr	316SS	75	9.3	38.5	50.8
J559	U-10Zr	316SS	75	9.2	38.5	50.8

The M-Series involved four TOP tests (M1–M4) conducted on eleven 316SS clad U-5Fs pins and three tests (M5–M7) conducted on six D9/HT9 clad U-19Pu-10Zr/U-Zr pins irradiated in flowing sodium loops in the TREAT facility, as shown in Table 3 [41]. Tested pins varied from fresh fuel to high-burnup (9.8 at.%) samples and were subject to an 8-s transient up to approximately four times the nominal power to establish a comprehensive report of modern metallic-fuel behavior under severe accident conditions. Some tests were stopped just before pin failure while others were halted just after pin breach. Specifically, the objectives of the test series were determining cladding-failure thresholds, identifying mechanisms driving pin failure, understanding transient fuel behavior (e.g. fuel melting), and quantifying the negative-feedback mechanism of axial fuel elongation for a wide range of fuel burnups [42]. M1 was primarily focused on initial observations of transient-induced fuel extrusion [43]. In-reactor fuel motion was monitored during the transient using TREAT’s hodoscope capabilities, giving detailed calculations of axial fuel-column growth [44]. M2–M4 showed the high propensity for axial growth demonstrated by U-5Fs during transient conditions following fuel melting. During these tests, researchers implemented several design changes to improve representativeness of experiment to actual SFR conditions and found pin failure to be caused primarily by the formation of the low-melting-point eutectic at the fuel-cladding interface. Additionally, pin failure was further aggravated by RIP. M5–M7 tests showed a significant portion of fuel for each pin underwent melting during the transient and was expelled during pin breach. Also, the modern ternary and binary fuels displayed less axial growth than U-Fs, which was attributed to a higher operating temperature, leading to less retained fission gas [45,46]. M7 was also significant because it was the first TOP test of its kind to test U-10Zr and newly elected cladding of choice, HT9. The U-10Zr pin from M7 remained intact throughout the transient overpower (up to 4.8 times nominal power) with a transient-induced cladding wastage layer extending only about one third of the way into the cladding. While the M-Series provided invaluable insight into transient behavior of metallic fuels, it was limited in the number of samples tested, thus complicating the ability to identify and generalize correlations between burnup, composition, pre-failure axial expansion, and pin failure.

Table 3. M-Series pin specifications and test parameters.

Test ID	Comp.	Clad	Peak BU (at.%)	Smear Dens. (% theor.)	Power at Termination or Failure	Pin Failure	Axial Swelling (%)
M-2	U-5Fs	316 SS	0.3	75	4× nom. power	No failure	16
M-2	U-5Fs	316 SS	4.4	75	4× nom. power	Top of fuel column	15
M-2	U-5Fs	316 SS	7.9	75	4× nom. power	Top of fuel column	3
M-3	U-5Fs	316 SS	0.3	75	3.8× nom. power	No failure	18
M-3	U-5Fs	316 SS	4.4	75	3.8× nom. power	No failure	4
M-3	U-5Fs	316 SS	7.9	75	3.8× nom. power	No failure	4
M-4	U-5Fs	316 SS	Fresh	75	4.1× nom. power	No failure	3
M-4	U-5Fs	316 SS	2.4	75	4.1× nom. power	Top of fuel column	-
M-4	U-5Fs	316 SS	4.4	75	4.1× nom. power	No failure	4

Test ID	Comp.	Clad	Peak BU (at.%)	Smear Dens. (% theor.)	Power at Termination or Failure	Pin Failure	Axial Swelling (%)
M-5	U-19Pu-10Zr	D9	0.8	72.5	4.4× nom. power	No failure	2–3
M-5	U-19Pu-10Zr	D9	1.9	72.5	4.2× nom. power	No failure	2–3
M-6	U-19Pu-10Zr	D9	1.9	72.5	4.2× nom. power	No failure	4
M-6	U-19Pu-10Zr	D9	5.3	72.5	4.1× nom. power	Top of fuel column	4
M-7	U-19Pu-10Zr	D9	9.8	72.5	4.0× nom. power	Top of fuel column	2–3
M-7	U-10Zr	HT9	2.9	72.5	4.8× nom. power	No failure	8–9

1.3. THOR-C-2 Background and Motivation

To address needs to continue nuclear heated-safety research and transient testing of modern reactor fuels, the TREAT facility officially restarted in 2017 and planned to revive the planned M-8 experiment to be housed in a newly designed sodium-environment module, the Transient Heat sink Overpower Response (THOR) capsule [47]. The THOR capsule was developed to measure time-dependent thermal behavior of SFR and light-water reactor fuel pins subjected to accident conditions within TREAT [48]. The THOR-commissioning tests were devised to establish the performance of the test device and explore fresh metallic fuel performance. These tests will determine the capsule’s capacity to measure and detect the behavior of fresh SFR fuel during severe accident conditions, including heat-sink temperature near the fuel pin and time of clad rupture. THOR-C-2 was irradiated in TREAT in August 2022 and contained an unirradiated EBR-II Mk-IV fuel pin that experienced severe TOP conditions, establishing both a tie-back case to historical testing and power-coupling measurements for calorimetric calibration factors for metallic fuels [48,49].

1.4. THOR-M-TOP-1 Background and Motivation

Historical research conducted on metallic fuel pins has indicated that the mode of failure depends on the fuel composition, burnup, and irradiation history of the fuel pins. Expanded efforts are needed to accurately predict and quantitatively delimit the thresholds between failure mechanisms to inform safety criteria for SFRs. A recent review of research demands for SFR fuels identified many research gaps to aid in demonstrating the full safety envelope of HT9-clad metallic fuels, including the demand for transient testing of high-burnup ($10 < BU < 20$ at.%) and ultra-high -burnup (> 20 at.%) metallic fuels [50,51]. The THOR-Metallic campaign aims to validate and expand historical TOP and LOF testing on high-burnup U-Zr and U-Pu-Zr fuel alloys previously irradiated in EBR-II by running the rods to failure [52]. Results from THOR-M will aid in validating fuel-performance models and establishing safety criteria for licensing. THOR-M-TOP will examine the influence of thermal creep on pin failure under transient-overpower conditions, as conceptualized in M-8.

The pins selected for the test and sibling pin for THOR-M-TOP-1 were chosen based on their composition, cladding, irradiation histories, and plenum geometries to optimize observation of high-temperature thermal creep behavior [53]. Both pins are high-burnup U-19Pu-10Zr and have a low plenum-to-fuel volume ratio, resulting in decreased fission-gas accommodation, aggravated FCMI, and overall conservative transient response when compared to modern U-Zr pin designs with larger plenum-to-fuel ratios[3,54]. DP 40, the chosen test pin of THOR-M-TOP-1 and previous candidate for M8, and DP 36, its sibling pin, were retrieved from the reserve of EBR-II spent fuel pins at the Radioactive Scrap and Waste Facility (RSWF) and transferred to the Hot Fuel Examination Facility (HFEF). Both pins contain ternary, U-Pu-Zr, fuel, which has demonstrated more-limiting behaviors than binary, U-Zr fuel, providing a conservative estimation of failure thresholds. Both pins are also clad in HT9 and have been irradiated in EBR-II to a peak burnup of over 11 at.%. Finally, both pins have a plenum-to-fuel volume

ratio of 1.1, which is below the suggested standard for metallic fuel-pin fabrication, but will yield necessary RIP. Relevant information for the pins can be found in Table 4.

Table 4. THOR-MTOP-1 and sibling pin test matrix.

Test ID	Exp. ID	Pin ID	Comp	P/F vol.	Sm. Dens.	BU	Clad type
THOR-M- TOP-1	X441A	DP 40	U-19Pu-10Zr	1.1	75	11.1	HT9
Sibling	X441A	DP 36	U-19Pu-10Zr	1.1	75	11.6	HT9

2. SUMMARY OF PRE-TRANSIENT CHARACTERIZATION, EXPERIMENTS, AND IRRADIATION HISTORY

2.1. Pre-Transient Characterization

The pre-transient characterization efforts for THOR-M-TOP-1 have included non-destructive examination (NDE) on both DP 40 and DP 36, including visual inspection, neutron radiography, dimensional inspection through contact profilometry, and precise gamma spectrometry. DP 36 has been analyzed using destructive examination (DE) techniques through plenum gas puncturing for FGR quantification and sectioning for optical microscopy in order to establish a pre-transient baseline for comparison with the DE results from DP 40 post-transient, as summarized in Table 5. These examinations will establish a baseline for steady-state fuel behavior, establish a pre-transient baseline for comparisons with post-transient characterization, identify anomalous pin features, and verify pre-irradiation pin integrity. Additionally, results will supplement the database of historically characterized pre-irradiated EBR-II pins.

Table 5. Summary of Pre-Transient Characterization Completed on DP 40 and DP 36.

Examination	X441A-DP 40	X441A-DP 36
Visual	X	X
Neutron radiography	X	X
Profilometry	X	X
Gamma scan	X	X
Gas Assay, Sample and Recharge	—	X
Sectioning and Optical Microscopy	—	X

2.2. Experiment Description and Sample Information

2.2.1. THOR-C-2 Irradiation Plan

The metallic fuel alloy was cast into quartz molds using an injection-casting system to draw the alloy melt into the mold. The Mk-IV fuel pin consists of U-10Zr metallic fuel slugs, sodium bond, HT9 cladding, and inert-gas plenum. The main characteristics are reported in Table 6. The planned approach of post-transient characterization revealed detailed behavior of U-10Zr under intermediate transient conditions. The approximate power conditions experienced during the THOR-C-2 irradiation in TREAT are shown in Figure 1. The fresh U-10Zr pin was loaded into the instrumented THOR capsule, where the pin is sodium bonded to a Ti heat sink to create the desired thermal-boundary conditions for the test. Throughout the transient, the *in situ* capsule instrumentation recorded thermal measurements, fuel motion, and pin failure through thermocouples, a linear variable differential transformer (LVDT), and an acoustic-emission sensor (AES), respectively. The capsule underwent intermediate TOP conditions, intended to evoke pin failure, within the THOR capsule in TREAT. Post-irradiation neutron tomography has been conducted, and analysis of the results will be provided in this report.

Table 6. Geometry and specifications for Mk-IV fuel pin used in THOR-C-2.

THOR-C-2	
Composition	U-10Zr
Fuel length (nominal)	34.3 cm
Element length (nominal)	74.7 cm
Fuel Diameter	4.3 mm
Cladding	HT-9
Cladding OD	5.8 mm
Cladding thickness	0.45 mm
Plenum / Fuel vol	1.45
Smear density	75%
Plenum gas	He
Initial Fill Gas Pressure	0.1 MPa at RT
Heat Sink Material	Ti64

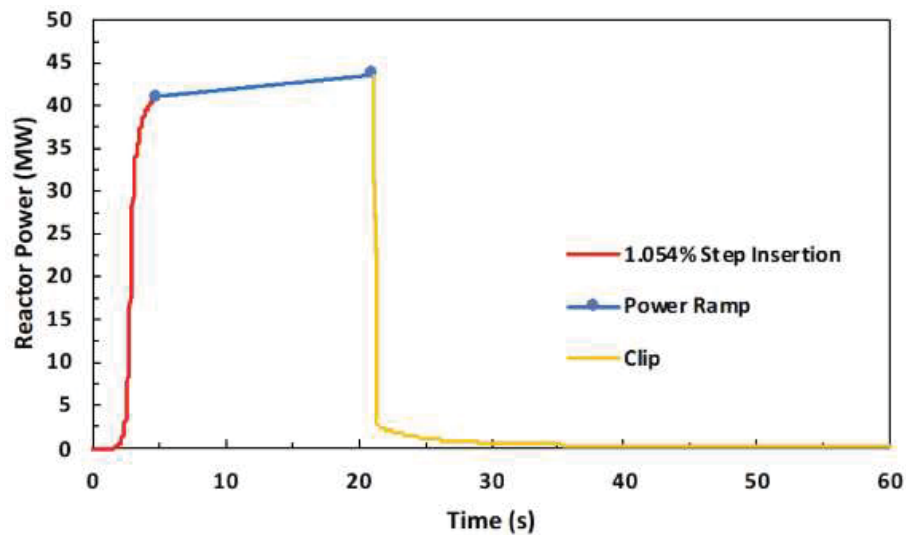


Figure 1. Targeted transient for the THOR-C-2 experiment in the TREAT facility [47].

2.2.2. THOR-M-TOP-1 Irradiation Plan

The metallic fuel alloys were cast into quartz molds using an injection-casting system to draw the alloy melt into the mold [25,54]. Both Mk-III pins consist of sodium-bonded metallic fuel slugs, HT9 cladding, and inert-gas plenums. Both pins were previously irradiated in EBR-II as part of the X441A experiment [3,5]. Full geometry specifications and burnup are listed in Table 7. A planned approach of pre- and post-transient characterization will reveal detailed behavior of U-19Pu-10Zr under TOP conditions. Pin X441A-DP 40 will be loaded into the instrumented THOR capsule, where the pin is sodium bonded to a Ti heat sink to create the desired thermal boundary conditions for the test. Throughout the planned transient, the *in situ* capsule instrumentation will be recorded. It includes thermocouples to record thermal measurements, along with an LVDT to measure fuel-pin axial elongation and an AES to identify pin failure or breach. DP 40 will undergo anticipated intermediate TOP conditions typical for an SFR within the in the TREAT reactor. The transient conditions are comparable to those of

THOR-C-2, but they will not be a direct corollary. DP 36 will serve as the sibling pin for pre-transient destructive analysis. Post-irradiation neutron radiography has previously been conducted for both DP 40 and DP 36 during the X441A campaign. This report will also compare the newly acquired neutron-radiography data with historical results.

Table 7. Geometry and specifications for DP 40 and DP 36.

	X441A-DP 40	X441A-DP 36
Composition	U-19Pu-10Zr	U-19Pu-10Zr
Fuel length (nominal)	34.3 cm	34.3 cm
Element length (nominal)	74.9 cm	74.9 cm
Fuel Diameter	4.39 mm	4.39 mm
Cladding	HT-9	HT-9
Cladding OD	5.84 mm	5.84 mm
Cladding thickness	0.38 mm	0.38 mm
Plenum / Fuel vol	1.1	1.1
Smear density	75%	75%
Plenum gas	75% He + 25% Ar	75% He + 25% Ar
Tag gas	Xe	Xe
Peak Burnup Reached	11.1 (at.%)	11.6 (at.%)
Heat Sink Material	Ti64	Ti64

3. NON-DESTRUCTIVE EXAMINATION RESULTS AND DISCUSSION

3.1. Visual Inspection

Visual inspections of the selected pins were conducted, and digital images were taken through the hot-cell windows of HFEF with no anomalous observations or defects, as is evident in the example image in Figure 2a. Pins were identified by the labeling located on the bottom end caps. Modifications made to the pins include outfitting them with end fittings to facilitate transportation and maneuverability within the hot cell. To ensure no corrosion occurred during the 36 years in which the pins were stored, the wire wrap was removed from each pin, and the outer cladding was inspected using the visual-examination machine (VEM). No evidence of outer corrosion was observed as seen in an example VEM image (Figure 2b).

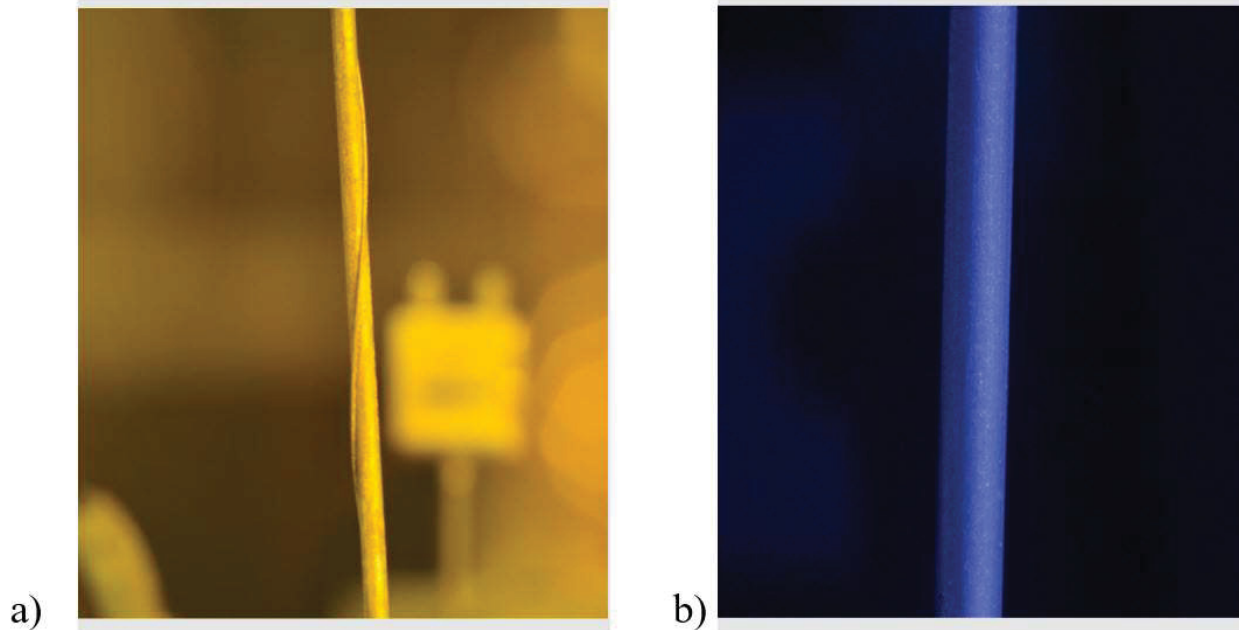


Figure 2. Through-window visual image of DP 40 with wire wrap (left) and VEM image of DP 40 without wire wrap (right).

3.2. Neutron Radiography

Neutron radiography was performed using the Neutron Radiography Reactor (NRAD) located in the basement of HFEF. The NRAD reactor is a 250 kW Training Research Isotope General Atomics reactor with two beam lines. The east beam line is uniquely capable of imaging irradiated materials because it services a position below the main floor of the hot cell, which is where pins DP 36 and 40 were loaded. Neutrons pass through the fuel specimen and expose different activation foils. Neutron-radiography images were taken from the pins at two or three angles (0 and 90 degrees or 0, 120, and 240 degrees) with both a dysprosium foil for thermal-neutron radiography and a Cd-covered indium foil for epithermal-neutron radiography. The rotations were fixed by placing the rodlets in a collet to fix the radial position. The radiographs from the two and three angles are very similar, revealing no major non-axisymmetric features. The foils were approximately 43 cm in length, requiring two iterations of shots to image the entire length of the pins.

Thermal neutron radiographs of the examined fuel pins (Figure 3) confirmed typical metallic-fuel behaviors—the fuel appears to have swollen radially, eliminating the fuel-cladding gap, and small amounts of fuel and/or fission products show a cloudy, porous (~40% mass fraction [55,56]) presence in the sodium at the top of the pin plenum due to fuel-sodium bond interaction, fission-product solubility in sodium, and extrusion of the bond to the plenum. The fluff structures can be seen in both pins in Figure 3 and Figure 4; however, the fluff structure of DP 40 is dispersed farther up the plenum. The mechanisms and variables affecting the formation of the fluff structure are currently under investigation [55,56]. Fuel-stack liftoff is another potential feature that could be present in metallic fuel post-irradiation [57]; however, neither pin confirmed this behavior. Quantitative measurements of the fuel-pin dimensions and features were achieved using the MATLAB image-analysis plug-in and the visible calibrated scale marked with Gd paint located on the imaging vehicle.

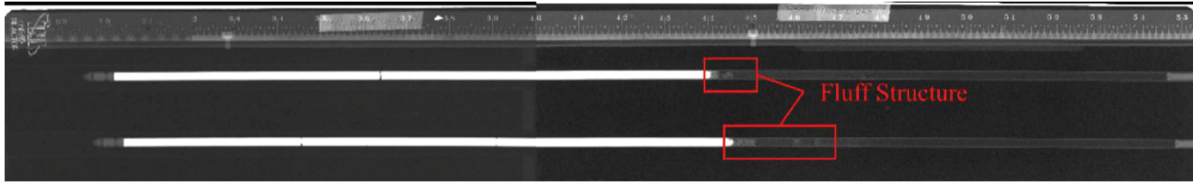


Figure 3. Thermal neutron radiography of the fuel elements DP 36 (top) and DP 40 (bottom).

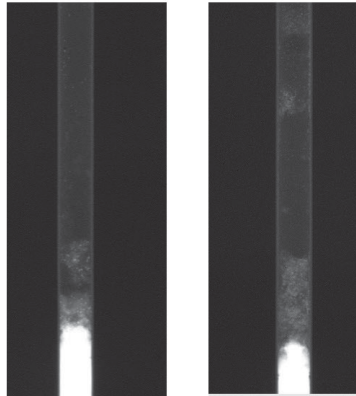


Figure 4. Thermal neutron radiograph of low-density and fluff-structure regions at the tops of the fuel columns of DP 36 (left) and DP 40(right).

The axial elongation of the fuel columns in DP 40 and DP 36 are reported in Table 8. The fuel column of DP 40 measured approximately 3.65% longer compared to as-fabricated dimensions and meets expectations for a ternary metallic-fuel pin of comparable burnup; however, the axial growth measured in DP 36 is only about 2.15%, which is consistent with historically determined values of 1.5–4.0% for ternary fuel irradiated to approximately 11 at.% [54]. Additionally, these recorded fuel-column length measurements vary only slightly from measurements from previously acquired neutron radiography from DP 1 post-transient analysis, as shown in Table 8.

Table 8. Measured axial growth for Pins DP 40 and DP 36.

Fuel Pin ID	Peak BU (at%, calculated)	Axial Growth from Original Neutron Radiograph (NR)	Axial Growth from Newer NR
X441A-DP 40	11.1%	4.37%	3.65%
X441A-DP 36	116%	1.95%	2.15%

3.3. Dimensional Inspection

Dimensional inspections of both fuel pins were conducted using the HFEF element contact profilometer, bow, and length machine to analyze outer-cladding deformation. The wire wrap was removed from each pin, and linear scans of the pins were performed in roughly axial 0.127 cm increments and rotating the pin at four angles, spaced 45 degrees apart. The resulting axial diametral profiles for DP 40 and DP 36, illustrated in Figure 5, show greatest cladding deformation along the lower half of the fuel column due to fuel swelling. Additionally, the end cap welds are observable as large-diameter spikes toward the bottom of the pin.

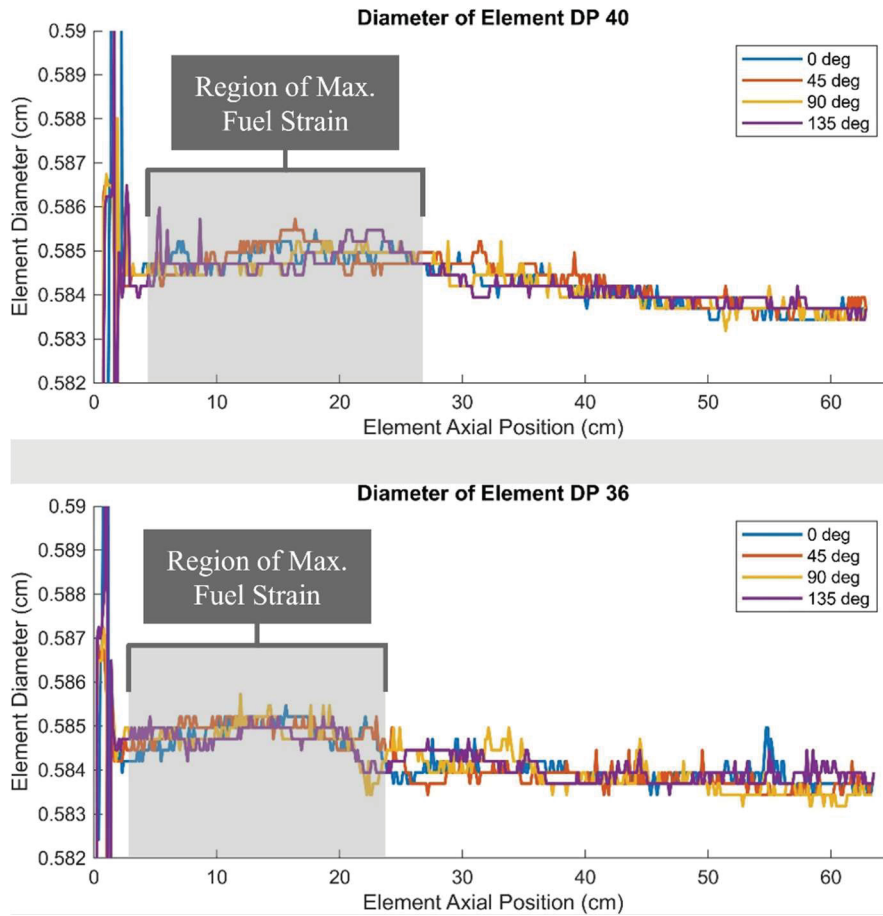


Figure 5. Diametral measurements from element contact profilometry for DP 40 (top) and DP 36 (bottom). Axial position is measured from the bottom of the fuel pin.

Quantitative comparison between the measured diameter and as-fabricated cladding outer diameter showed a maximum strain of 0.34% and 0.30% for DP 40 and DP 36, respectively (Table 9). FCMI-induced strain is of particular concern when dealing with high-burnup samples (>10 at.%) due to the accumulation of solid fission products, but the cladding strain is mild for these high-burnup pins, well within the experimental range for HT9-clad U-Pu-Zr irradiated up to ~11 at.% [54].

Table 9. Maximum cladding deformation measured via contact profilometry.

Fuel Pin ID	Peak BU (at.% calculated)	Cladding Type	Max Clad Strain
X441A-DP 40	11.2%	Re	0.34 %
X441A-DP 36	11.6%	HT-9	0.30 %

3.4. Gamma Spectrometry

Gamma-ray spectrometry of both fuel pins was performed using the HFEF PGS. The PGS has three major components: collimator, stage, and detector. The collimator penetrates the HFEF cell wall with a rectangular aperture that is adjustable from 0.254 to 0.00254 cm in height and is 2.2225 cm wide. The collimator can be rotated from horizontal to vertical orientation. The stage manipulates the sample in front of the collimator in the plane facing it and can rotate the sample about its central axis. The detector consists of a Compton suppressed high-purity germanium detector, and its control system moves the stage and collimator and initiates the scans.

Both pins were stored for more than 30 years after they were last irradiated, so the only remaining detectable isotope (above background radiation) was the relatively long-lived radionuclide Cs-137. Figure 6 shows the Cs-137 gamma spectra of DP 40 and DP 36, axially aligned with the neutron-radiography image of the pins.

In metallic fuel, Cs isotopes produced by fission are often dissolved in the Na bond between the fuel and the cladding. As the fuel swells, some sodium permeates the pores of the fuel, but a large portion is extruded from the annular space between fuel and cladding to the gas plenum. The Cs migrates with the Na above the fuel column, producing a Cs activity spike above the fuel, as can be seen in Figure 6. Some Cs-137 signal “undulation” along the fuel stack can be potentially related to features (e.g., cracks, slug interfaces) visible from neutron radiography.

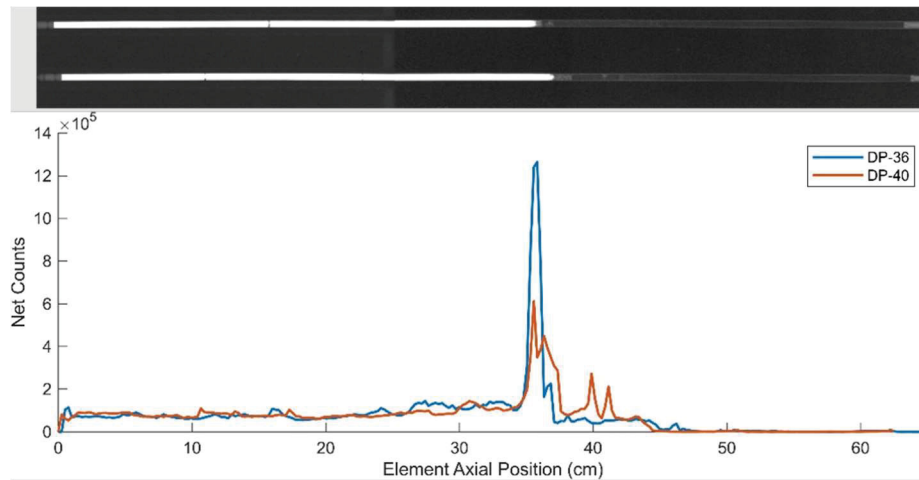


Figure 6. Axial distribution of Cs-137 as detected by gamma scan, overlaid with neutron radiographs of X441A-DP 36 (top) and X441A-DP 40 (bottom).

4. DESTRUCTIVE EXAMINATION RESULTS AND DISCUSSION

4.1. Fission-Gas Release

Fission gases were collected from pin DP 36 using the HFEF Gas Assay, Sample, and Recharge (GASR) system. The plenum was punctured using a 150 W Nd-YAG laser system, the initial gas pressure was recorded, and a sample of expelled fission gases was collected. The void volume was then measured by recording expansions into the GASR system following controlled backfills into the plenum puncture. From there, the internal gas pressure was determined using the initial gas pressure and void volume. Fission-gas analysis is typically performed using gas mass spectrometry data and an assumed number of fissions attributed to U-235, U-238, Pu-239, and Pu-240. Mass spectrometry conducted on the gas sampled from the plenum puncture of DP 36 has not yet been completed; therefore, GASR analysis will be resumed upon receipt of the mass-spectrometry data.

4.2. Sectioning

After performing GASR as described in the previous section, pin DP 36 was sectioned through the fuel zone at different axial positions to investigate the evolution of microstructure and thermal diffusivity with the axial and radial temperature distribution. Radial and longitudinal cross-sections about 6 mm (radial) and 10 mm (longitudinal) long were cut, mounted in epoxy, and polished to a 0.25 μm finish. Additional samples were taken from three different axial positions along the fuel stack and sent to the INL Analytical Laboratory for a variety of chemical and radiological analyses. The primary goals of these examinations were burnup determination and thermal-diffusivity measurement. The cutting plan for the DP 36 fuel pin is shown in Figure 7, along with the position and thickness of each sample for microscopy, burnup analysis, and laser flash analysis (LFA). Results from the thermal-diffusivity and burnup measurements are not yet available.

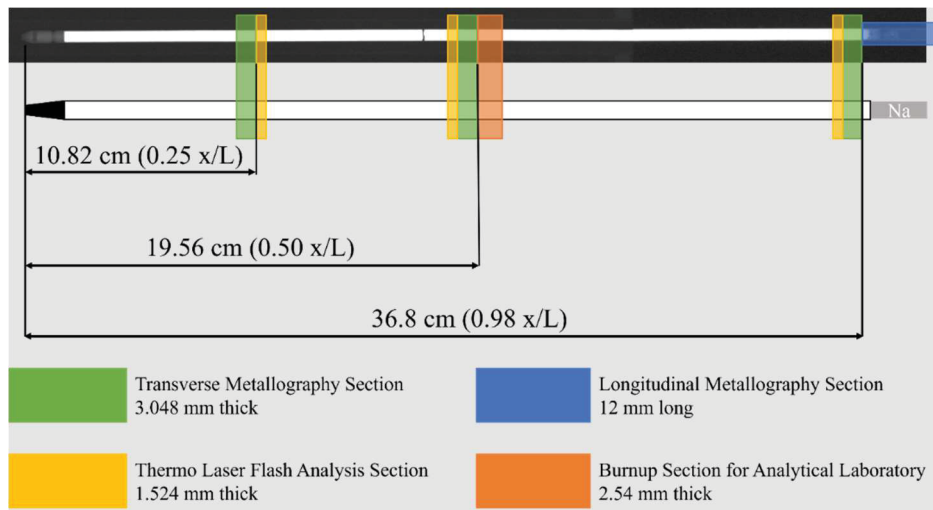


Figure 7. DP 36 fuel-pin cutting diagram, describing the different sample configurations, purposes, and axial positions.

4.3. Metallography

Optical microscopy was performed on a Leica DMI8 inverted microscope at INL HFEF using different magnification lenses capable of resolving the microstructures at different degrees of detail for different axial positions along the fuel element.

During irradiation, U-Zr and U-Pu-Zr fuel slugs are known to undergo restructuring. Radial thermal gradients alter Zr solubility and mobility within the fuel matrix, resulting in a migration of Zr to the

central and outer radial regions in U-Pu-Zr [58]. At operating temperatures of greater than 650°C at the central region of the fuel, a Zr-rich, porous, body-centered cubic (bcc)- γ phase is formed [38]. Temperatures between 600–650°C have been reported for the mid-radial region, where dense, intermediate $\gamma + \zeta$ phases were present. At the fuel periphery, temperatures between 500–600°C resulted in $\delta + \zeta$ phases and increased porosity. While refractory data and phase identification have not been completed on the samples, it is conjectured that the same behavior is present within the fuel pin based on visually distinguishable oxidized regions. The suspected regions and fission-gas bubble formation are most evident at 0.5x/L for X441A-DP 36, as labeled in the transverse cross section in Figure 8b and Figure 8e. At 0.25x/L, initial constituent redistribution is observed, although it is less distinct than seen at 0.5x/L (Figure 8a and Figure 8d). Also, at the lower axial position, a central void appears to have formed, which has been historically attributed to material becoming dislodged during sample preparation or to thermal and swelling stresses at low burnups, expected to diminish with increasing burnup and fuel swelling [59]. Both transverse and longitudinal cross-sections at 0.98x/L were also examined (Figure 8c and Figure 8f), revealing the low-density fuel-sodium interaction region at the top of the fuel column.

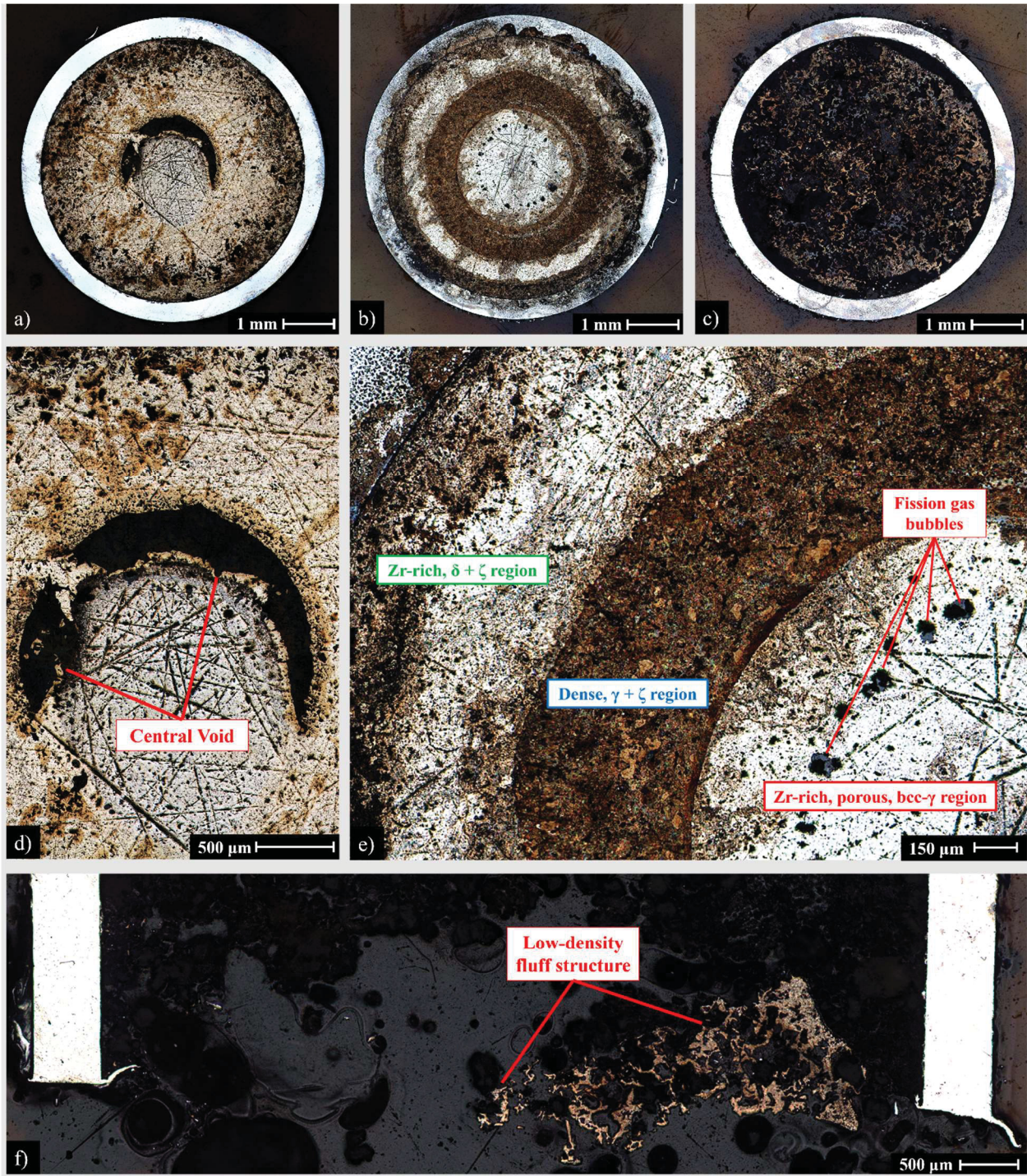


Figure 8. Transverse optical metallography cross-sections of X441A-DP 36 taken at (a) 0.25x/L, (b) 0.50x/L, and (c) 0.98x/L. Further magnified images of (d) 8a and (e) 8b, showcasing important microstructural features, and (f) a longitudinal optical metallography cross section taken at 0.98x/L.

5. POST-TRANSIENT ANALYSIS OF COMMISSIONING TOP TEST

5.1. Neutron Computed Tomography

Following transient irradiation, the THOR-C-2 capsule was imaged using neutron radiography and x-ray radiography at TREAT. The radiography identified two primary regions of interest (ROIs) near the top and bottom of the fuel column. These specific areas were examined at NRAD's North Radiography Station using neutron-computed tomography (nCT). Digital neutron radiographs were taken at various angles and reconstructed into three-dimensional (3D) visualizations of both ROIs with a spatial resolution of approximately 52.9 μm . Using FIJI software, 3D projections of the lower and upper ROIs were generated from the raw nCT data, as seen in Figure 9a and Figure 10a, respectively. Using identifiable features from INL Drawing 822806, a scale was established to conduct dimensional analysis on the structural features of the failed fuel pin, including cladding deformation and relocated fuel. During the transient test, the sample underwent fuel melting, cladding breach, central-void formation, and fuel relocation. Examples of each feature captured via radiograph are shown in Figure 11.

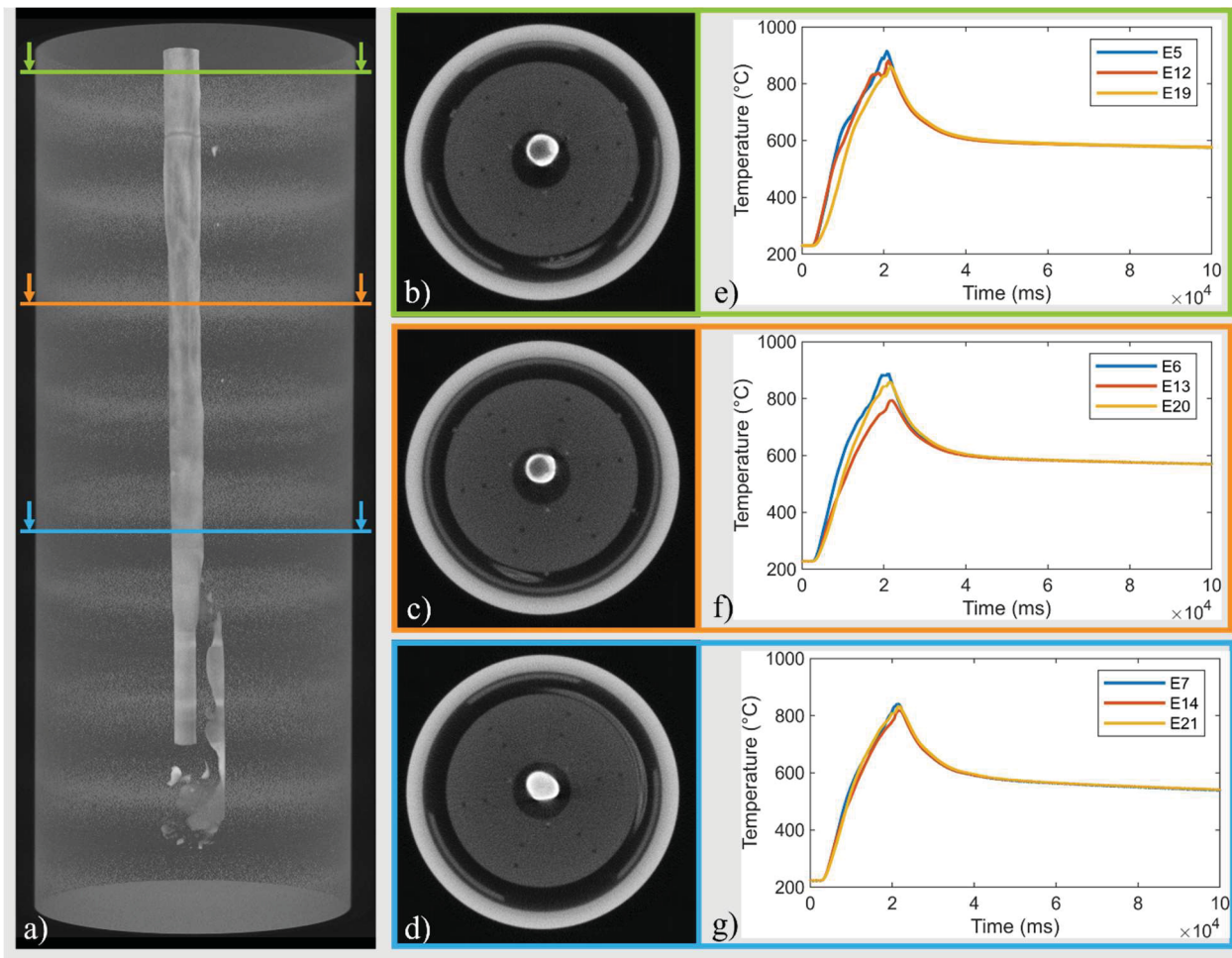


Figure 9. 3D nCT projection of the lower region of interest for THOR-C-2 (a), individual nCT slices showing three thermocouple placements within the Ti heatsink at each of the axial positions (b) 4.1 cm, (c) 8.3 cm, and (d) 12.5 cm, and accompanying heat sink temperatures measured from TCs at axial positions (e) 4.1 cm, (f) 8.3 cm, and (g) 12.5 cm.

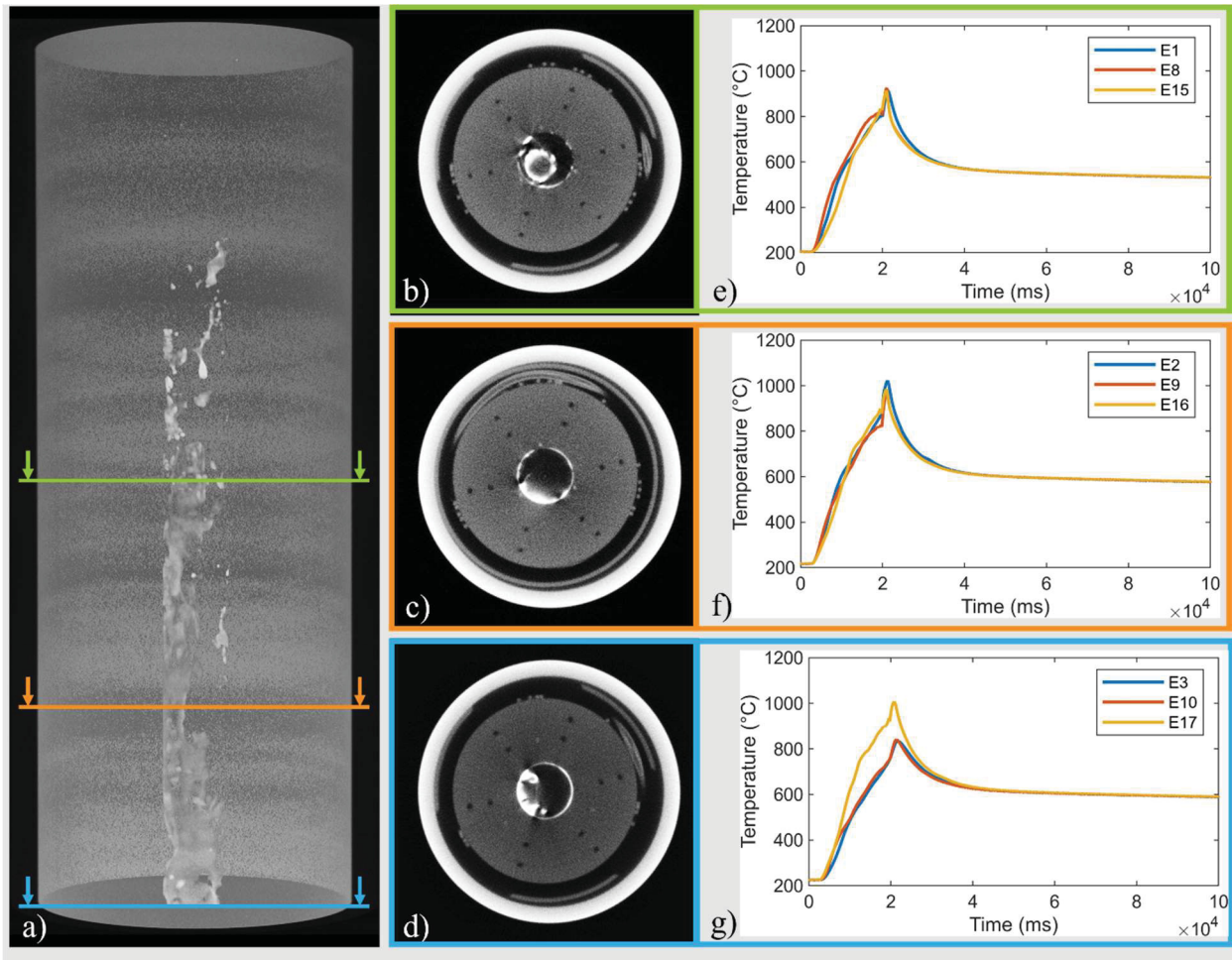


Figure 10. 3D nCT projection of the upper region of interest for THOR-C-2, (a) individual nCT slices showing three thermocouple placements within the Ti heatsink at each of the axial positions (b) 29.7 cm, (c) 25.4 cm, and (d) 23.9 cm, and accompanying heat sink temperatures measured from the TCs at axial positions (e) 29.7 cm, (f) 25.4 cm, and (g) 21.1 cm.

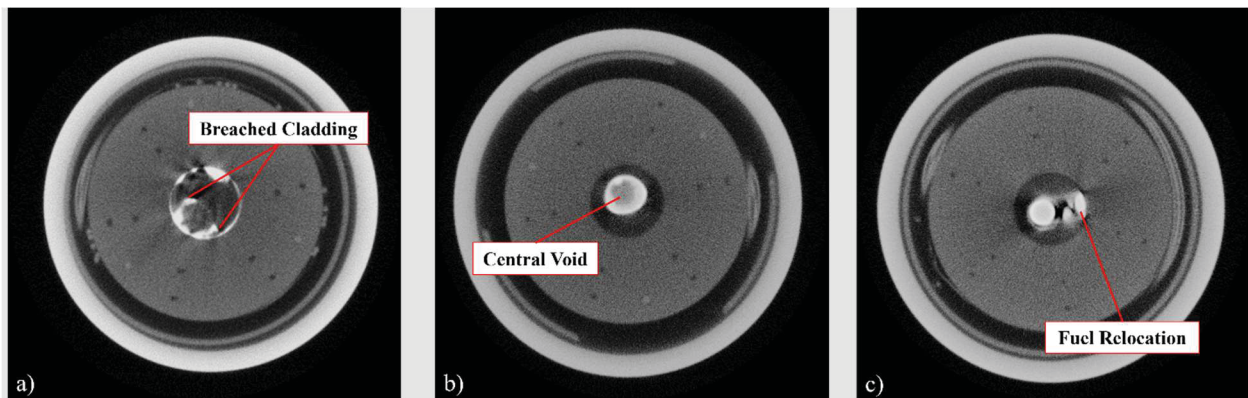


Figure 11. Transverse nCT radiographs showing breached cladding at (a) 30.0 cm, (b) central void at 5.3 cm, and © relocated fuel at 0.7 cm above the beginning of the fuel column.

Cladding burst is evident in the nCT slices from approximately 29.2 cm above the bottom of the fuel column to the lower boundary of the radiograph at approximately 23.9 cm. Melted fuel was expelled from the pin, and it collected along the side of the cladding (an event known as candling) and in the bottom of the capsule. The candling of the relocated fuel can be seen primarily from 2.2 cm above the bottom of the fuel column until the bound of the lower ROI radiograph at approximately 13.5 cm above the bottom of the fuel column. Fuel also collected at the bottom of the capsule’s fuel-pin chamber from about 2.1 to 0.9 cm below the bottom of the fuel column. A redistribution of fuel along one side of the heatsink wall from 0.9 cm below the bottom of the fuel column extending approximately 4.6 cm, axially. The relocated fuel left behind a central void within the fuel pin, evident from approximately 4.9 to 5.9 cm from the bottom of the fuel stack.

Cladding diameter along the radiographed regions was initially measured using the image processor, FIJI, and results of calculated strain are shown in Figure 12. As was seen in results from pre- and post-transient analysis, cladding strain was greatest along the lower region of the fuel pin. Difficulties in analyzing the nCT radiographs for cladding diameter arose in differentiating the outer cladding surface from the relocated fuel deposited on the clad exterior along a large portion of the fuel pin and establishing an accurate scale, given limited features of known length. Results can be compared with future dimensional analysis from DEs following disassembly of the capsule for accuracy. Planned work includes conducting systematic cladding strain and mass fraction measurements along the entirety of the imaged ROIs using machine learning and segmentation techniques. Quantifying these behaviors is essential to understanding the transient behavior of fuel and compiling an adequate safety envelope for fuel-system qualification.

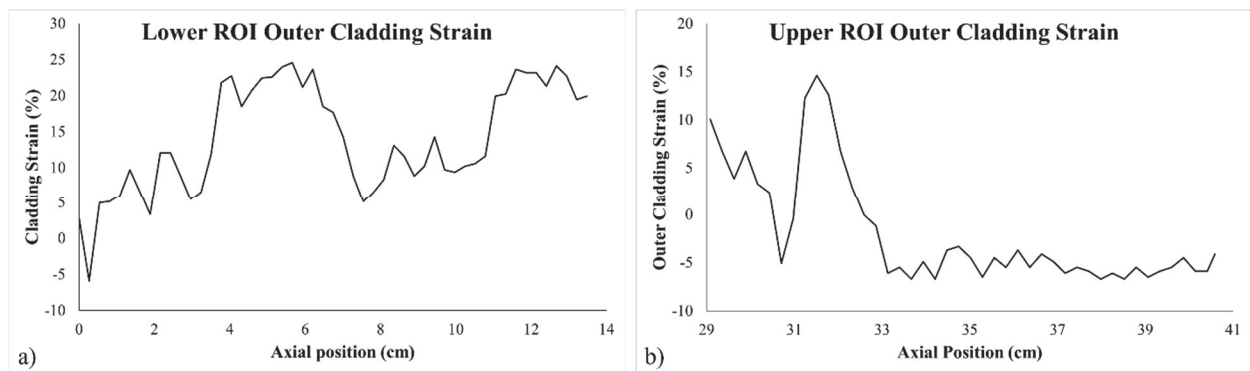


Figure 12. Cladding strain measurements from nCT for (a) the lower and (b) upper ROIs.

5.2. Thermal Measurements

The THOR capsule was instrumented with 21 (three bundles of seven) Type-K thermocouples (TCs) fitted in predrilled holes into the Ti heat sink. These provided *in situ* measurement of temperature throughout the irradiation of THOR-C-2. While the axial position of each TC was determined using the as-built data package, INL Drawing 822806, and INL Drawing 822799, no distinguishable features indicate the orientation of the capsule to definitively differentiate between the three TCs at a given axial location. For the lower ROI, the nCT images where the TCs penetrated most deeply into the heatsink and were, therefore, in the closest position to the fuel pin were found to be at approximately 4.1, 8.3, and 12.5 cm above the bottom of the fuel column, as shown in Figure 9a–d. The corresponding thermal readings throughout the transient are also shown in Figure 9e–g. The temperature of this region of the pin rose quickly during the transient, reaching temperatures between 795 and 915°C by the end of the transient. These temperatures are measured inside the heatsink, a small distance from the fuel pin, but still create a significant delay and lower temperature measurement compared to the actual fuel temperatures. The bias of these measurements will be reported by future analysis. Still, these values already exceed reported values for some of the eutectic formations in the fuel-cladding system [35,36]. The thermal

measurements demonstrate increasing cladding temperatures at higher axial positions along the fueled element. As previously mentioned, the identity of the TCs at each axial position could not be determined, but an informed conjecture can be made based on the features visible in the nCT image at the axial position. In Figure 9d and Figure 11g, TC E13 recorded lower values than the other TCs at the same height, which could be attributed to the asymmetry of the fuel pin causing TC E13 to be the furthest from the pin.

The same procedure was applied to the upper ROI. However, only two nCT images contained the images of the closest TC locations to the pin. Figure 10a–c show the positions and nCT slices at 29.7 and 25.4 cm above the bottom of the fuel column. The lowest nCT image is included in Figure 10d at approximately 23.9 cm to inform potential features occurring at the actual TC axial position of 21.1 cm above the bottom of the fuel stack. The nine highest TCs measured temperatures up to 834–1023°C during the transient, as seen in Figure 10e–g, which again can surpass the liquidus temperature of the fuel. Like previous efforts to address anomalous behavior, examining structural features in Figure 10d could provide explanation why TC E17 in Figure 10g displayed significantly higher temperatures than the other TCs at the same height and help to assign TC identities. Overall, *in situ* thermal measurements contributed to understanding of fuel response under TOP conditions and will provide key information into temperature-related lifetime limiting phenomena in future testing. Further evaluation of temperature measurement bias will provide more accuracy for fuel temperatures during the transient.

6. FUTURE WORK

While post-transient neutron radiography was collected for the THOR-C-2 pin and capsule, further examination will require disassembly within the hot cell for both NDE and DE. Planned NDE includes two-dimensional NR and VEM. Destructive analysis will require sectioning the pin for dimensional measurements, followed by mounting and preparation for optical and scanning electron microscopy. Additionally, a computational approach is recommended to systematically examine the structural features of the failed fuel pin. Using machine-learning segmentation techniques, relocated fuel can be massed and tracked.

Ongoing objectives for THOR-M-TOP-1 include completing the destructive pre-transient analysis for DP 36 and irradiating and examining pin DP 40. The sampled fission gas from the puncture sampling will be sent to Pacific Northwest National Laboratory for analysis, and the received data will be used to finish fission-gas-release calculations. Additionally, planned thermal-diffusivity measurements and burnup analysis will be conducted at the Analytical Laboratory at MFC, according to the sectioning diagram in Figure 7. Pin DP 40 will undergo an intermediate transient within the THOR capsule in the TREAT reactor to simulate conditions representative of a TOP in an SFR. In-pile fuel motion will be monitored using TREAT's Fuel Motion Monitoring System, expanding further understanding of axial elongation under accident conditions. Additionally, post-transient analysis will include neutron radiography, element-contact profilometry (ECP), PGS, GASR, optical metallography, scanning electron microscopy, electron probe micro-analysis, burnup and fuel isotopic analysis, and bulk thermal-property measurements. The results will be compared to the baseline established with sibling pin DP 36, and distinct conclusions can be drawn regarding transient behavior of metallic fuel during a TOP occurrence.

7. CONCLUSIONS

The Advanced Fuels Campaign has supported the continuation of SFR metallic-fuel safety testing through the THOR campaign conducted within the TREAT facility. Available characterization data for the THOR-C-2 and THOR-M-TOP-1 experiment have been analyzed in this report. THOR-C-2 successfully demonstrated the transient testing and instrumentation capabilities of the THOR capsule. Post-transient nCT conducted on the THOR-C-2 capsule, alongside planned NDE and DE, will aid in establishing a comprehensive understanding of fresh U-10Zr behavior during TOP conditions, including the pins' surface temperature during the transient, cladding deformation, and fuel relocation. In addition

to providing a tie-back case to historical TOP testing, THOR-C-2 also provides power-coupling calibration factors for intermediate transients conducted with irradiated fuel, such as THOR-M-TOP-1. These results will contribute to further analytical evaluations of the fuel performance, using fuel performance codes, to more provide needed validation data to support further development of transient fuel performance models.

THOR-M-TOP-1 will use two high-burnup U-19Pu-10Zr pins, previously irradiated in EBR-II experiment X441A. One will serve as the test pin to be irradiated within TREAT, and the other as a sibling pin for pre-transient characterization. Both pins were confirmed to be intact through VEM. Further NDE was conducted on both pins to identify any anomalous features developed during steady-state testing. Axial fuel elongation and cladding strain were quantified through neutron radiography and ECP, and all measurements were found to be consistent with reported values for pins of similar burnup and composition. Gamma scanning of both pins also showed the mobilization of Cs-137 to the top of the fuel column. Finally, DEs of the sibling pin helped establish a baseline of steady-state behavior for comparison to post-transient analysis of the test pin. Supplementary DE to be conducted includes thermal-diffusivity and burnup testing.

THOR-M-TOP-1 is planned to undergo an intermediate transient—representative of a TOP occurrence in an SFR environment—within TREAT. Post-transient analysis will include neutron radiography, nCT, PGS, ECP, sectioning, optical microscopy, LFA, and burnup analysis to extensively characterize the transient response of high-burnup U-19Pu-10Zr. The results will then be compared to data from the sibling pin and other characterized pins from EBR-II.

8. ACKNOWLEDGEMENT

This work was supported by the Advanced Fuels Campaign. Also, HFEF operations and process engineers are acknowledged for the different analysis and measurements performed and data acquisition for the engineering scale post-irradiation examination.

9. REFERENCES

1. Aitkaliyeva, A. 2022. “Recent trends in metallic fast reactor fuels research.” *Journal of Nuclear Materials* 558: 153377. <https://doi.org/10.1016/j.jnucmat.2021.153377>.
2. Carmack, W. J., *et al.*, 2009. “Metallic fuels for advanced reactors.” *Journal of Nuclear Materials* 392(2): 139–150. <https://doi.org/10.1016/j.jnucmat.2009.03.007>.
3. Crawford, D. C., D. L. Porter, and S. L. Hayes. 2007. “Fuels for sodium-cooled fast reactors: US perspective.” *Journal of Nuclear Materials* 371(1–3): 202–23. <https://doi.org/10.1016/j.jnucmat.2007.05.010>.
4. Walters, L. C., J. H. Kittel, and B. R. Seidel. 1984. “Performance of metallic fuels and blankets in liquid-metal fast breeder reactors.” *Nuclear Technology* 65(2): 179–231. <https://doi.org/10.13182/NT84-A33408>.
5. Tsai, H. and M. C. Billone. 1987. “Data Package for The Irradiation of The DP 1 Test (X441) in EBR-II.” Argonne National Laboratory, Lemont, IL.
6. Seidel, B., *et al.* 1990. “A Decade of Advances in Metallic Fuel.” In proceedings of the American Nuclear Society winter meeting, Washington, DC, November 11–15. https://inis.iaea.org/collection/NCLCollectionStore/_Public/22/038/22038427.pdf?r=1.
7. Hofman, G. L. 1980. “Irradiation Behavior of Experimental Mark-II Experimental Breeder Reactor II Driver Fuel.” *Nuclear Technology* 47(1): 7–22. <https://doi.org/10.13182/NT80-A32408>.
8. Walter, C., G. Golden, and N. Olson. 1975. “U--Pu--Zr metal alloy: a potential fuel for LMFBR's.” <https://doi.org/10.2172/7138403>.

9. Leggett, R. and L. Walters. 1993. "Status of LMR fuel development in the United States of America." *Journal of Nuclear Materials* 204: 23–32. [https://doi.org/10.1016/0022-3115\(93\)90195-5](https://doi.org/10.1016/0022-3115(93)90195-5).
10. Puigh, R. J., and G. G. Wire. 1983. "In-reactor creep behavior of selected ferritic alloys." In proceedings of the TMS/AIME Topical on Ferritic Alloys for Use in Nuclear Energy Technologies, May 19–23, Snowbird, UT. Westinghouse Hanford Co., Richland, WA. https://inis.iaea.org/collection/NCLCollectionStore/_Public/15/022/15022240.pdf?r=1.
11. Gelles, D. 1987. "Effects of irradiation on ferritic alloys and implications for fusion reactor applications." *Journal of Nuclear Materials* 149(2): 192–199. <https://www.sciencedirect.com/science/article/pii/0022311587904776>.
12. Pahl, R. G., W. N. Beck, and J. E. Sanecki 1987. "Postirradiation examination of the HT9 clad fuel test X425 at 2.9% burnup." ANL-IFR-81, Argonne National Laboratory, Lemont, IL. <https://doi.org/10.2172/713968>.
13. Pahl, R. G., C. E. Lahm, and G. D. Hudman. 1985. "Test description for the Integral Fast Reactor subassemblies X419, X420, and X421." ANL-IFR-19, Argonne National Laboratory, Lemont, IL. <https://doi.org/10.2172/711870>.
14. Hwang, W., H. Y. Kang, C. Nam, and J. O. Kim. 1997. "Design characteristics of metallic fuel rod on its in-LMR performance." Korea Atomic Energy Research Institute. <https://www.osti.gov/etdeweb/servlets/purl/598983>.
15. Hofman, G. L., R. Pahl, C. Lahm, and D. Porter. 1990. "Swelling behavior of U-Pu-Zr fuel." *Metallurgical Transactions A* 21: 517–528. <https://link.springer.com/content/pdf/10.1007/BF02671924.pdf>.
16. Walters, L. 1999. "Thirty years of fuels and materials information from EBR-II." *Journal of Nuclear Materials* 270(1-2): 39–48. [https://doi.org/10.1016/S0022-3115\(98\)00760-0](https://doi.org/10.1016/S0022-3115(98)00760-0).
17. FRWG. 2018. "Nuclear Metal Fuel: Characteristics, Design, Manufacturing, Testing, and Operating History." In White Paper 18-01 for the nuclear Regulatory Commission. Fast Reactor Working Group. <https://www.nrc.gov/docs/ML1816/ML18165A249.pdf>.
18. Pitner, A., and R. Baker. 1993. "Metal fuel test program in the FFTF." *Journal of Nuclear Materials* 204: 124–130. [https://doi.org/10.1016/0022-3115\(93\)90208-G](https://doi.org/10.1016/0022-3115(93)90208-G).
19. Porter, D. L., and H. Tsai. 2012. "Full-length U-xPu-10Zr (x=0, 8, 19wt.%) fast reactor fuel test in FFTF." *Journal of Nuclear Materials* 427(1–3): 46–57. <https://doi.org/10.1016/j.jnucmat.2012.03.047>.
20. Cohen, A. B., H. Tsai, and L. A. Neimark. 1993. "Fuel/cladding compatibility in U-19Pu-10Zr/HT9-clad fuel at elevated temperatures." *Journal of Nuclear Materials* 204: 244–251. [https://doi.org/10.1016/0022-3115\(93\)90223-L](https://doi.org/10.1016/0022-3115(93)90223-L).
21. Carmack, W. J., et al. 2020. "Examination of Legacy Metallic Fuel Pins (U-10Zr) Tested in FFTF." INL/EXT-20-28987, Idaho National Lab, Idaho Falls, ID. https://inldigitallibrary.inl.gov/sites/sti/sti/Sort_24588.pdf.
22. Carmack, W. J., H. M. Chichester, D. L. Porter, and D. W. Wootan "Metallography and fuel cladding chemical interaction in fast flux test facility irradiated metallic U-10Zr MFF-3 and MFF-5 fuel pins." *Journal of Nuclear Materials* 473: 167–177. <https://doi.org/10.1016/j.jnucmat.2016.02.019>.
23. Grabaskas, D. 2010. "Analysis of Transient Overpower Scenarios in Sodium Fast Reactors." Thesis, Nuclear Engineering Graduate Program. The Ohio State University, Columbus, OH.

https://etd.ohiolink.edu/acprod/odb_etd/ws/send_file/send?accession=osu1265726176&disposition=inline.

24. Drzewiecki, T., J. Schmidt, C. VanWert, and P. Clifford. 2022. "Fuel Qualification for Advanced Reactors." NUREG-2246, U.S. Nuclear Regulatory Commission, Washington, DC. <https://www.nrc.gov/docs/ML2206/ML22063A131.pdf>.
25. Hofman, G. L., L. C. Walters, and T. Bauer. 1997. "Metallic fast reactor fuels." *Progress in Nuclear Energy* 31(1-2): 83–110. [https://doi.org/10.1016/0149-1970\(96\)00005-4](https://doi.org/10.1016/0149-1970(96)00005-4).
26. Carmack, W., et al. 2009. "Metallic fuels for advanced reactors." *Journal of Nuclear Materials* 392(2): 139–150. <https://doi.org/10.1016/j.jnucmat.2009.03.007>.
27. Batté, G., and G. Hoffman. 1990. "Run-Beyond-Cladding-Breach (RBCB) test results for the Integral Fast Reactor (IFR) metallic fuels program." In proceedings of the International topical meeting on fast reactor safety Conference, Snowbird, UT, August 12-16. Argonne National Laboratory, Lemont, IL. <https://www.osti.gov/biblio/7176746>.
28. Buzzell, J., G. Hudman, and D. Porter. 1981. "Transient performance of EBR-II driver fuel." Argonne National Laboratory, IL (USA); Argonne National Laboratory, Lemont, IL. <https://digital.library.unt.edu/ark:/67531/metadc1210605/>.
29. Planchon, et al. 1986. "The experimental breeder reactor II inherent shutdown and heat removal tests—results and analysis." *Nuclear Engineering and Design* 91(3): 287–296. [https://doi.org/10.1016/0029-5493\(86\)90082-8](https://doi.org/10.1016/0029-5493(86)90082-8).
30. Sumner, T. S., and T. Y. Wei. 2012. "Benchmark specifications and data requirements for EBR-II shutdown heat removal tests SHRT-17 and SHRT-45R." ANL-ARC-226, Argonne National Laboratory, Lemont, IL (United States). <https://doi.org/10.2172/1432465>.
31. Liu, Y. Y., et al. 1993. "Behavior of EBR-II Mk-V-type fuel elements in simulated loss-of-flow tests." *Journal of Nuclear Materials* 204: 194–202. [https://doi.org/10.1016/0022-3115\(93\)90217-M](https://doi.org/10.1016/0022-3115(93)90217-M).
32. Janney, D. E., S. L. Hayes, and C. A. Adkins. 2019. "A Critical Review of the Experimentally Known Properties of U-Pu-Zr Alloys. Part 1: Phases and Phase Diagrams." *Nuclear Technology* 205(11):1387–1415. <https://doi.org/10.1080/00295450.2019.1578573>.
33. Janney, D. E., S. L. Hayes, and C. A. Adkins. 2020. "A critical review of the experimentally known properties of U-Pu-Zr alloys. Part 2: thermal and mechanical properties." *Nuclear Technology* 206(1): 1–22. <https://doi.org/10.1080/00295450.2019.1623617>.
34. Janney, D. E., and S. L. Hayes. 2018. "Experimentally known properties of U-10Zr alloys: A critical review." *Nuclear Technology* 203(2): 109–128. <https://doi.org/10.1080/00295450.2018.1435137>.
35. ASM Handbook. 2016. "Fe (Iron) Binary Alloy Phase Diagrams." *Volume 3 Alloy Phase Diagrams*, Edited by H. Okamoto, M.E. Schlesinger, and E.M. Mueller. ASM International. <https://doi.org/10.31399/asm.hb.v03.a0006162>.
36. Hwang, W., C. Nam, B. O. Lee, and W. S. Ryu. 1998. "Experimental Specifications for Eutectic Reaction between Metallic Fuel and HT-9." Korea Atomic Energy Research Institute. Taejon, Republic of Korea. http://inis.iaea.org/search/search.aspx?orig_q=RN:30053459.
37. Sohn, Y. H., et al. 2000. "Analysis of constituent redistribution in the γ (bcc) U–Pu–Zr alloys under gradients of temperature and concentrations." *Journal of Nuclear Materials* 279(2-3) 317–329. [https://doi.org/10.1016/S0022-3115\(99\)00290-1](https://doi.org/10.1016/S0022-3115(99)00290-1).

38. Kim, Y. S., G. L. Hofman, S. L. Hayes, and Y. H. Sohn. 2004. “Constituent redistribution in U–Pu–Zr fuel during irradiation.” *Journal of Nuclear Materials* 327(1): 27–36. <https://doi.org/10.1016/j.jnucmat.2004.01.012>.
39. Hofman, G., S. Hayes, and M. Petri. 1996. “Temperature gradient driven constituent redistribution in U–Zr alloys.” *Journal of Nuclear Materials* 227(3): 277–286. [https://doi.org/10.1016/0022-3115\(95\)00129-8](https://doi.org/10.1016/0022-3115(95)00129-8).
40. Wachs, D. M., L. Capriotti, and D. Porter. 2021. “Behavior of metallic fast reactor fuels during an overpower transient.” *Journal of Nuclear Materials* 557: 153304. <https://doi.org/10.1016/j.jnucmat.2021.153304>.
41. Bauer, T. H., et al. 1990. “Behavior of Modern Metallic Fuel in TREAT Transient Overpower Tests.” *Nuclear Technology* 92(3): 325–352. <https://doi.org/10.13182/NT92-325>.
42. Rhodes, E., et al. 1990. “Transient feedback from fuel motion in metal IFR (Integral Fast Reactor) fuel.” In proceedings of International topical meeting on fast reactor safety Conference, Snowbird, UT, August 12–16. Argonne National Laboratory, Lemont, IL. https://inis.iaea.org/search/search.aspx?orig_q=RN:21076292.
43. Wright, A., C. Tomchik, and H. Connaway. 2020. “Transient Testing of Nuclear Fuels Performed in the Original Operation of TREAT (First Edition).” ANL-ART-186, Argonne National Laboratory, Lemont, IL. <https://doi.org/10.2172/1595326>.
44. Rhodes, E. A., et al. 1992. “Fuel Motion in Overpower Tests of Metallic Integral Fast Reactor Fuel.” *Nuclear Technology* 98(1): 91–99. <https://doi.org/10.13182/NT92-A34653>.
45. Bauer, T., et al. 1989. “First overpower tests of metallic IFR [Integral Fast Reactor] fuel in TREAT [Transient Reactor Test Facility]: Data and analysis from tests M5, M6, and M7.” ANL-IFR-124, Argonne National Laboratory, Lemont, IL. <https://doi.org/10.2172/714655>.
46. Tomchik and A. Wright. 2023. “Benchmark Specifications for TREAT Tests M5, M6, and M7.” ANL-ART-174, Argonne National Laboratory, Lemont, IL. <https://doi.org/10.2172/1924431>.
47. Jensen, C., et al. 2023. “THOR-M Post Transient Examination Plan.” PLN-6705, Idaho National Laboratory, Idaho Falls, ID.
48. Imholte, D., et al. 2020. “Temperature Heat Sink Overpower Response (THOR) Module.” CDR-196, Idaho National Laboratory, Idaho Falls, ID.
49. INL. 2023. “Temperature Heat Sink Overpower Response (THOR) Capsule Commissioning Test Series.” TFR-1073, Idaho National Laboratory, Idaho Falls, ID.
50. Walters, L. et al. 2012. “Sodium Fast Reactor Fuels and Materials: Research Needs.” SAND2011-6546, Sandia National Laboratories, Albuquerque, NM. <https://doi.org/10.2172/1044975>.
51. Denman, M., et al. 2012. “Sodium Fast Reactor Safety and Licensing Research Plan-Volume I.” SAND2012-4260, Sandia National Laboratories, Albuquerque, New Mexico. <https://doi.org/10.2172/1044972>.
52. Imholte, D., et al. 2022. “THOR-Based EPIC and THOR-M Experiments.” Technical and Functional Requirements, Materials and Fuels Complex, Idaho National Laboratory, Idaho Falls, ID.
53. Capriotti, L. 2022. “Pre-transient Characterization of the AFC Metallic fuel pins for Safety Testing.” Idaho National Laboratory, Idaho Falls, ID.
54. Ogata, T. “3.01 - Metal Fuel.” in *Comprehensive Nuclear Materials* 3: 1–40. <https://doi.org/10.1016/B978-0-08-056033-5.00049-5>.

55. Di Lemma, F. G., et al. 2021. "Investigation of fuel microstructure at the top of a metallic fuel pin after a reactor overpower transient." *Journal of Nuclear Materials* 544: 152711. <https://doi.org/10.1016/j.jnucmat.2020.152711>.
56. Fay, J., et al. 2022. "An analysis of fluff formation in metallic fuel via data analyzes from EBR-II experiments and BISON fuel code modeling." *Journal of Nuclear Materials* 567(15): 153813. <https://doi.org/10.1016/j.jnucmat.2022.153813>.
57. Porter, D. L., G. L. Hofman, B. R. Seidel, and L. C. Walters. 1986. "Factors Controlling Metal Fuel Lifetime." In proceedings of the International conference on reliable fuels for liquid metal reactors. Tucson, AZ, September 7. <https://www.osti.gov/servlets/purl/6891881>.
58. Janney, D. E., and C. Papesch. 2017. "Metallic Fuels Handbook, Part 1: Alloys Based on U-Zr, Pu-Zr, U-Pu, or U-Pu-Zr, Including Those with Minor Actinides (Np, Am, Cm), Rare-earth Elements (La, Ce, Pr, Nd, Gd), and Y; and Part 2: Elements and Alloys not Based on U-Zr, Pu-Zr, U-Pu, or U-Pu-Zr." INL/EXT-15-36520, Idaho National Laboratory, Idaho Falls, ID. <https://doi.org/10.2172/1504934>.
59. Seidel, B. R., L. C. Walters, and Y. I. Chang. 1987. "Advances in metallic nuclear fuel." *JOM* 39: 10–13. <https://doi.org/10.1007/BF03258852>.